Biomacromolecules

Article

Cite This: Biomacromolecules 2018, 19, 1175−1188

pubs.acs.org/Biomac

Designing Highly Thermostable Lysozyme−Copolymer Conjugates: Focus on Effect of Polymer Concentration

Chandan Kumar Choudhury,[†] Sidong Tu,[†] Igor Luzinov,[†] Sergiy Minko,[‡] and Olga Kuksenok*[,†]

[†]Department of Materials Science and Engineering, Clemson University, Clemson, South Carolina 29634, United States

[‡]Nanostructured Materials Laboratory, The University of Georgia, Athens, Georgia 30602, United States

Supporting Information

ABSTRACT: Designing biomaterials capable of functioning in harsh environments is vital for a range of applications. Using molecular dynamics simulations, we show that conjugating lysozymes with a copolymer [poly(GMA-*stat*-OEGMA)] comprising glycidyl methacrylate (GMA) and oligo(ethylene glycol) methyl ether methacrylate (OEGMA) results in a dramatic increase of stability of these enzymes at high temperatures provided that the concentration of the copolymer in the close vicinity of the enzyme exceeds a critical value. In our simulations, we use triads containing the same ratio of GMA to OEGMA units as in our recent experiments (N. S. Yadavalli et al., *ACS Catalysis*, **2017**, *7*, 8675). We focus on the dynamics of the conjugate at high temperatures and on its structural stability as a function of the copolymer/water content in the vicinity of the enzyme. We show that the dynamics of phase separation in the water−copolymer mixture surrounding the enzyme is critical for the structural stability of the enzyme. Specifically, restricting water access promotes the structural stability of the lysozyme at high temperatures. We identified critical water concentration below which we observe a robust stabilization; the phase separation is no longer observed at this low fraction of water so that the water domains promoting unfolding are no longer formed in the vicinity of the enzyme. This understanding provides a basis for future studies on designing a range of enzyme−copolymer conjugates with improved stability.

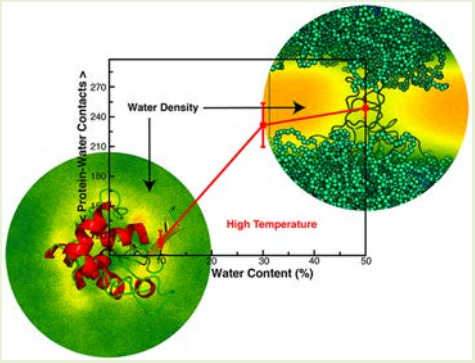

INTRODUCTION

Increasing stability of proteins with respect to diverse environmental conditions such as high temperature and various solvents is important for extending their use in various industrial and biomedical applications. Enzymes with enhanced thermal stability can remain catalytically active at temperatures inaccessible by native enzymes, offering biotechnological advantages by performing enzymatic reactions at high temperatures with higher reaction rates.[1,2] Improving thermal stability of enzymes could be beneficial for applications ranging from food processing[1] to deconstruction of biomass for biofuel industry.[3] Thermal stability of enzymes is also essential for enzyme enhanced oil recovery (EEOR) applications.[4−6] For example, thermostable and thermoactive enzymes called "breakers" are used to lower the viscosity of the fracturing fluid by hydrolyzing polymeric bonds and thus lowering viscosity of the solution in the deep wells.[4,5]

Enzyme stabilization is typically achieved either via the genetic mutations[7,8] or via conjugation of enzymes with solid substrates or other molecules.[9−19] In latter scenarios, the stability and activity of the resulting conjugate depends on the choice of chemical functionality of the monomer units, molecular weight of the polymer, and conjugation sites on the protein. For example, conjugating cationic polymers with lysozyme increases its activity, and this effect is attributed to the electrostatic attraction between the negatively charged cell wall and the positively charged lysozyme−polymer conjugate.[20] A number of studies showed that conjugation with poly(ethylene glycol) (PEG), or so-called PEGylation, can improve the stability of the secondary structures.[2,21−24] For example, Jain et al.[24] showed that oxygen in the PEG chain interacts strongly with the lysine residues and stabilizes the α-helical peptide. Further, it was also shown PEGylation reduces the solvent accessible surface area of the peptide, thus preventing the attack of water on the intrapeptide hydrogen bonds.[25] Similar observations were made for insulin−PEG conjugates.[23] It was also shown that PEGylation can result in mechanical reinforcement of peptides against the unfolding.[21] In the latter case, the mechanical reinforcement of a PEGylated peptide was attributed to the formation of an effective barrier formed by the PEG chains around the peptide with respect to the surrounding water molecules; this close proximity and high coverage of PEG chains with respect to the peptide surface reduces the probability of water molecules replacing the backbone H-bonds, which in turn prolongs the onset of unfolding events and stabilizes the helicity.[21]

PEGs are known to introduce molecular crowding which can affect the activity, structure, and dynamics of proteins. This

Received: January 6, 2018
Revised: March 12, 2018
Published: March 14, 2018

DOI: 10.1021/acs.biomac.8b00027
Biomacromolecules 2018, 19, 1175−1188

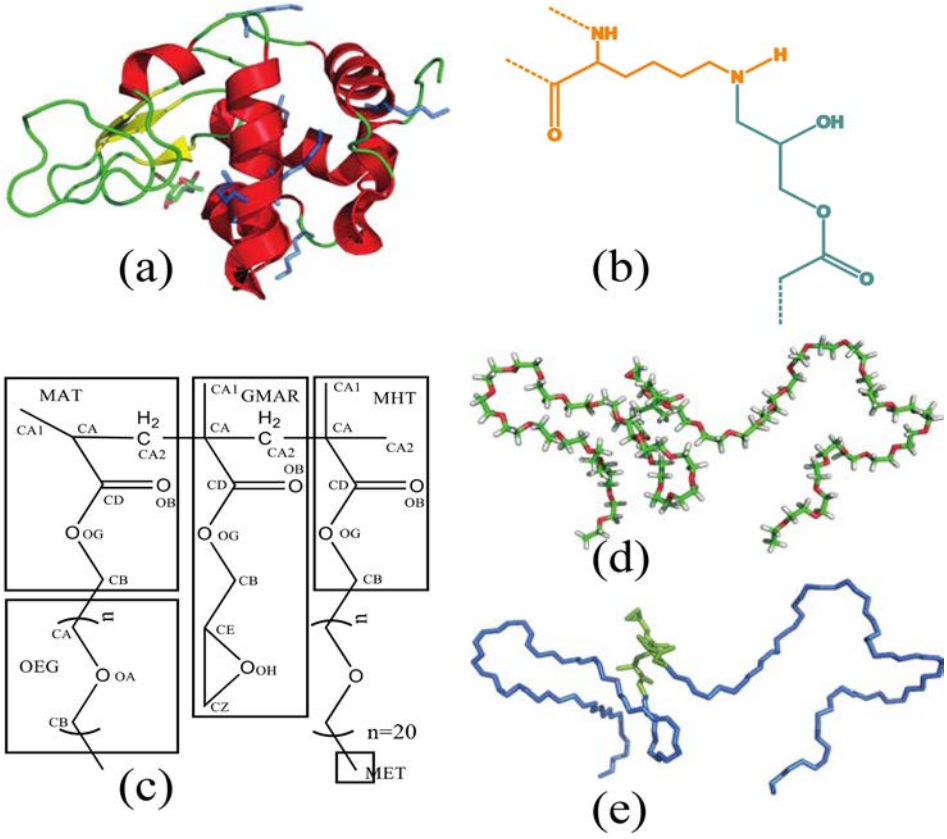

Figure 1. (a) 3-D representation of a lysozyme. Lysine residues are shown in blue and NAG is shown in green and red (stick representations). (b) Chemical structure of a conjugation point: lysine (in orange) is conjugated with GMA (in green). (c) Chemical structure of a triad. Twenty monomer units (n = 20) of PEG were constructed for each strand. (d) Atomic representation of a triad. Green, red, and white sticks are carbon, oxygen, and hydrogen atoms, respectively. (e) Triad is represented via hydrophilic (blue) and hydrophobic (green) segments. Hydrogens are not shown for clarity.

crowded environment can tune the interactions of protein with its surrounding thereby affecting protein folding and self-assembly.[26−29] While a number of studies suggest preferentially entropic stabilization of proteins by macromolecular crowders,[30,31] a few recent reports[32,33] show that the enthalpic interactions can provide a major contribution to the enzyme stabilization. Thus, both entropic[30,31] and enthalpic contributions and their interplay affect the stability of the conjugated enzyme. Further, when polymer is conjugated to a surface-tethered peptide, entropic contributions from steric interactions between the tethered polymer and a hard wall can result either in stabilization or destabilization of the secondary structures depending on the location of conjugation and a length of polymer chain.[34] Overall, the effect of PEGylation is site-specific and in general can lead to stability increase, decrease, or no significant outcome.[20,35−39] In addition, it was shown that excluding water around enzymes[25,40] or replacing it with various organic solvents[41] can lead to the dramatic improvement of their thermal stability.

In our recent study[42] that combined both experiments and simulations, we showed that the poly(GMA-*stat*-OEGMA) conjugated with lysozyme resulted in increasing the stability and maintaining activity of the enzyme well above 100 °C. In our experiments,[42] long copolymer chains were conjugated with the lysine residues of the lysozyme and formed cocoons enveloping the enzymes. These studies showed that the enzymes conjugated with copolymers remain permeable to the substrate during the studies of their activity. Note that the activity in the experimental studies was measured in two ways: at 45 °C after prior prolonged incubation at highly elevated temperatures and at elevated temperatures.[42] Our concurrent simulation results showed that at high temperatures the secondary structures of lysozyme conjugates were significantly more stable than that of the native lysozyme.[42] In the current work, we focus on understanding the underlying reason for this observed stabilization with poly(GMA-*stat*-OEGMA). To mimic the long copolymer chains used in our experiments, we use the triads containing the same ratio of GMA to OEGMA units as in our experiments.[42] We then conjugated six of these triads with all the lysine residues of the enzyme and in addition randomly placed free-floating triads within the simulation box (for details, see computation modeling section below).

In our simulations, we solely focus on assessing the structural stability at high temperatures and do not asses the functionality (activity) of the conjugates. A protein is considered stable if it retains structural integrity in response to various external stimuli.[43] When the system is driven out of equilibrium by various external stimuli including extreme temperatures, the slower the system reacts to the perturbing forces, the more stable is it.[43] The activity of the conjugated enzyme is preserved to a high degree after the prolonged heating as shown in our recent experimental studies.[42] Specifically, far UV circular dichroism (far UV CD) studies revealed substantial differences between the spectra of native enzymes and those of the enzymes conjugated with copolymer after they were subjected

DOI: 10.1021/acs.biomac.8b00027
Biomacromolecules 2018, 19, 1175−1188

Table 1. Simulation Details for Native Lysozyme and 0%, Case A (10% w/w), Case B (30% w/w), and Case C (50% w/w) LPC Systems[a]

	native	LPC			
		0%	case A (10% w/w)	case B (30% w/w)	case C (50% w/w)
triad chains	0	6 conjugated + 100 floating	6 conjugated + 100 floating	6 conjugated + 100 floating	6 conjugated + 100 floating
no. of water molecules	28 292	0	1472	5724	13 374
total no. of atoms	86 874	37 826	42 242	54 998	77 948
box dimensions (nm^3)	9.51 × 9.51 × 9.51	7.10 × 7.10 × 7.10	7.34 × 7.34 × 7.34	8.05 × 8.05 × 8.05	9.08 × 9.08 × 9.08

[a]Details are the same for 300 and 500 K.

to heating at high temperatures, and they showed significant stabilization of the secondary structures for the cases when enzyme was conjugated with the copolymer. Further, the α-helical content was also preserved to a significant degree in dehydrated lysozyme−polymer conjugate samples.[42] In addition, these studies showed a significant densification of the polymer cocoon around the enzyme.[42]

In the simulations below, we focus on the dynamics of the single enzyme at high temperature and on its structural stability as a function of the copolymer/water content in the vicinity of the enzyme.

METHODS

To understand the effect of concentration of triads on thermal stability of lysozyme−copolymer conjugates (LPC), we carried out molecular dynamics (MD) simulations of these conjugates at high temperatures and compared these studies with the native lysozyme at the same conditions as detailed below. The crystal structure of the native lysozyme from hen egg white (HEWL) was taken from RCSB protein data bank (http://www.rcsb.org, PDB ID: 3TXJ). HEWL structure was taken with the inhibitor, *N*-acetyl glucosamine (NAG) (Figure 1a). The position at which NAG binds to the enzyme indicates its active site. 3TXJ consists of 129 residues. Its secondary structure consists of six α-helices and three stranded antiparallel β-sheets (Figure 1a).

We simulated the HEWL (native) and HEWL with oligomer of poly(GMA-*stat*-OEGMA). Poly(GMA-*stat*-OEGMA) is a block copolymer of glycidyl methacrylate (GMA) and oligo(ethylene glycol) (Figure 1c,d). At an ambient temperature, oligo(ethylene glycol) is hydrophilic, while GMA is hydrophobic (Figure 1e). The CHARMM force fields[44−47] are employed for the protein and copolymer. The details of the force field parameters used are provided in the Supporting Information (Tables S1−S4)

Under the experimental conditions, the epoxy functional group of the triad reacts with the lysine residue of the lysozyme forming lysozyme−copolymer conjugate (LPC). This reaction results in formation of alkanolamine moiety as represented in Figure 1b; in our simulations, we conjugated all six lysine residues with the epoxy of the triad. The nitrogen of the amine side chain of the lysine reacts with the less substituted carbon of the epoxy, forming an alcohol and an amine group (Figure 1b). In the computational model, we created a bond between the nitrogen (lysine side chain) and the carbon (of the epoxy).[42] The dihedral parameters and the electronic charges for the atoms involved in bonding were developed[42] from the quantum chemical calculation using Gaussian 09 software;[48] these parameters are provided in Tables S1 of Supporting Information. The contour length of the long polymer chain in the experiments was 457 nm; this length significantly exceeds the size of our simulation box (7.36 nm). Further, a single long polymer chain creates covalent bonds with lysine residues of multiple enzymes, thereby simultaneously enveloping multiple enzymes.[42] In our simulations, we focus on the single enzyme conjugated with the small fraction of a much longer polymer chain. To account for the effects of enzyme interacting with the relatively long side chains grafted to the different segments of a polymer backbone, we add the free-floating triads and vary the polymer concentration to isolate a critical concentration promoting thermal stabilization. These free-floating triads play role of additional nonreacted side chains along the significantly longer copolymer molecular brush in our experiments.[42] This system is referred as LPC in this study. Corresponding to our experimental studies, we use 20 PEG monomer per triad strand (Figure 1c). Initially the solution of these triads dispersed in water (CHARMM TIP3P model[49]) was simulated for 50 ns before adding them to the lysozyme−water system.

We analyzed dynamics of the systems with three different concentrations of triads in water in both ambient (300 K) and high (500 K) temperatures. We fixed the number of free-floating triads (at a hundred triads) and varied the number of water molecules (and correspondingly the size of the simulation box) as listed in Table 1. It can be noted that the boiling point of water using original TIP3P water model is 593 K,[50] our simulation temperature is well below this boiling point. We use the CHARMM TIP3P water model,[49] which has slightly reduced bond and angle force constants. The NPT simulations at 300 K (pressure 1 bar) with CHARMM TIP3P water produces the density of 1005 kg m^{-3}. We then keep this water density throughout our NVT high temperature simulation runs. We note that this approach was used in a number of previous studies (high temperature NVT simulations with densities corresponding to ambient temperatures[23,51−53]). Notably, the CHARMM TIP3P water model produces unphysically low water density of 728 kg m^{-3} at high temperatures. The validity and limitations of using water at high temperatures are discussed in detail in ref 54.

Herein, we choose the systems with the three different concentrations of the copolymer in water that we refer to as case A (10% w/w of water), case B (30% w/w of water), and case C (50% w/w of water). In addition, we also simulated water-free lysozyme−copolymer complex. All the simulations were performed using GROMACS Molecular Dynamics package.[55,56] The crystal structure (PDBID:3TXJ) was solvated with CHARMM TIP3P[49] water model, and ions were added to neutralize the charges. CHARMM36 force fields[45] were employed for the enzyme and the inhibitor. The LPC−water systems were energy minimized through a combination of steepest descent and conjugate gradient minimization methods (as implemented in GROMACS). This structure was first subjected to the equilibration and then production runs. The simulation strategy is described in detail in the Supporting Information and in our previous work.[42]

The denaturation temperature of lysozyme (hen egg white) is about 350 K at pH 7.0.[57] To accelerate the unfolding process in our simulations, the system was heated to 500 K.[52,58,59] High temperature MD simulations are often used to accelerate unfolding of proteins,[51−53,58−74] which enable one to understand the structural transformation of protein to the random coil structure and in some cases to understand the fundamental principles of protein folding. For the two-state proteins, the transition state for folding and unfolding is expected to be the same from the principle of microscopic reversibility, which has been confirmed experimentally;[75] therefore, unfolding simulations give the structure of the folding transition state for two-state folding proteins as well as the unfolding transition state for multistate reactions.[73,76] It has also been shown that the high temperature simulations do not alter the pathway of the unfolding, but only its rate.[64]

DOI: 10.1021/acs.biomac.8b00027
Biomacromolecules 2018, 19, 1175−1188

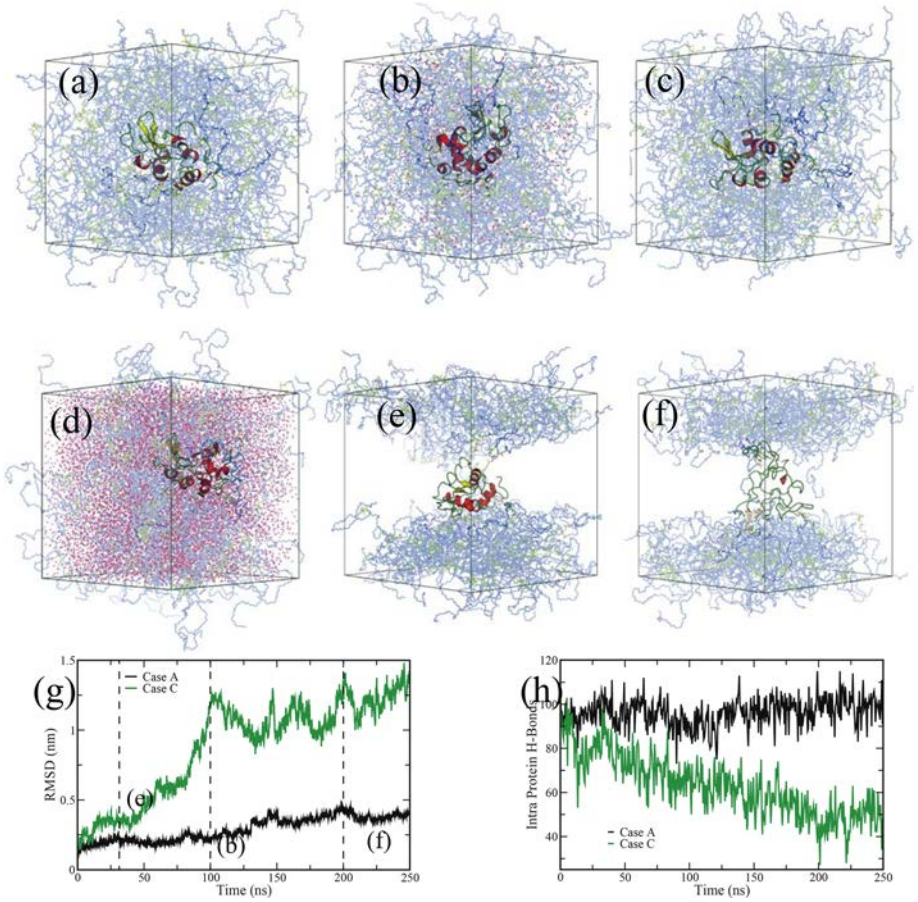

Figure 2. Time evolution of the LPC systems for case A (top panel) and case C (middle panel) at T = 500 K. (a) 0 ns, (b) 100 ns, and (c) 250 ns for case A; (d) 0 ns, (e) 30 ns, and (f) 200 ns for case C. Water molecules are not shown for clarity except in (d), where water molecules are shown in pink. (g) RMSD, (h) number of intraprotein H-bonds for case A and case C systems. Here, black and green lines are for case A and case C, respectively. Dashed lines in panel g marked b, e, and f correspond to the snapshots in panels b, e, and f.

With this approach, we capture the denaturation process of the native enzyme in agreement with the number of prior studies. For example, the unfolding characteristics of the native enzyme (R_g, RMSD, DSSP, a decrease in a total number of intraprotein hydrogen bonds) calculated in our high temperature simulations are in a good agreement with the respective prior simulation data (see, for example, refs 52, 59, and 77). In addition, it is known that PEG becomes hydrophobic at high temperatures[78−80] and hence undergoes aggregation. We capture this change in PEG affinity to water in our simulations (at 300 K, the triads are hydrophilic and are uniformly dispersed within the simulation box, while at 500 K, the triads become hydrophobic and aggregate).

All the simulations at 500 K were performed at a constant volume (NVT ensemble) corresponding to the density of the water model at 300 K.[23,51,52,58] Specifically, the 500 K simulations were initiated with the configuration obtained at the end of each 300 K simulations. Each simulation consisted of four sets with different initial velocities. We note that while either NVT[51,53,58,63,64,66,71−74] or NPT[81−83] ensembles are chosen in high temperature simulations, we have specifically chosen NVT ensemble, since this approach more closely corresponds to our experimental setup,[42] with the lysozyme−polymer conjugates heated within the container with the closed lid. Thus, in our NVT simulations, we keep the water density equal to that at 300 K.

RESULTS AND DISCUSSION

To understand the underlying reasons for the high thermal stability of lysozyme conjugated with poly(GMA-*stat*-OEGMA) observed in our experiments[42] and to potentially further optimize this system, we focus on the effects of concentration of triads on the unfolding process at high temperature. We increase the temperature of the system to 500 K and characterize the behavior of the LPC with respect to that of native lysozyme. As introduced above, we focus on three different concentrations of triads in this system: case A corresponds to the highest concentration of triads (10% w/w of water), and the remaining two cases correspond to the increase in water content, case B (30% w/w of water) and case C (50% w/w of water).

Examples of LPC Dynamics: High (Case A) and Low (Case C) Concentrations of Triads. In our first series of simulations shown in Figure 2, we focus on conformational changes in high temperatures in two cases, at the highest (case A, a−c in the top row) and at the lowest (case C, d−f in the middle row) triad concentrations considered in our simulations of LPC immersed into water. These snapshots show that while the secondary structures are preserved to a large degree for case A (Figure 2a−c) (both the α-helices and the β-sheets are conserved), the secondary structures are disrupted for case C. Figure 2e highlights the instant in time at which the phase-separation takes place and the enzyme is pulled into the water phase (at 30 ns). Our characterizations of this system provided below show that the instant in time when the enzyme is surrounded by water marks the onset of the unfolding process.

RMSD and Number of Intraprotein H-Bonds. To characterize the dynamics of this system quantitatively, we calculate the root−mean−square deviation (RMSD), which captures the

DOI: 10.1021/acs.biomac.8b00027
Biomacromolecules 2018, 19, 1175−1188

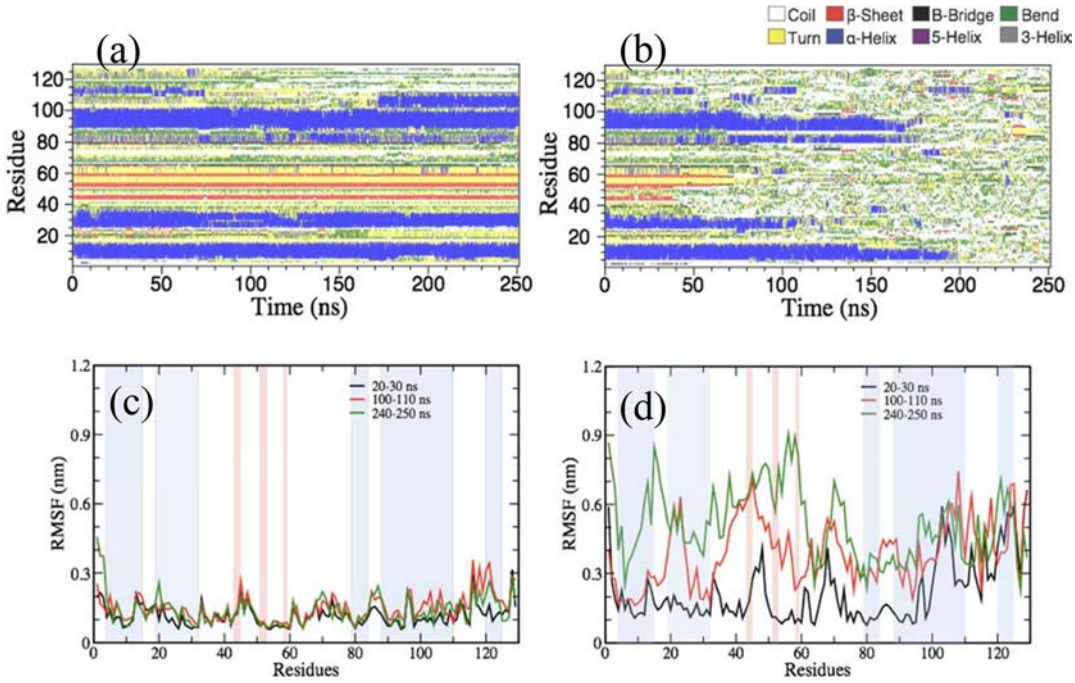

Figure 3. Time progression of (a, b) secondary structures and (c-d) root−mean−square fluctuation (RMSF). Left panel, case A; right panel, case C at 500 K. The shaded regions (in c and d) are the secondary conformations present in the crystal structure. The light blue shaded regions represent the α-helices and the light red regions represent β-sheets.

deviation of protein conformation from its initial conformation, and the number of intraprotein hydrogen bonds (H-bonds). Prior to calculating the RMSD, the rotational and translational superposition of the enzyme with respect to its initial structure (as defined in GROMACS) is performed. Then we calculate RMSD using backbone C_α atoms as

$$\mathrm{RMSD}(t) = \left[\frac{1}{N}\sum_{i=1}^{N}(\mathbf{r}_i(t) - \mathbf{r}_i(0))^2\right]^{1/2} \quad (1)$$

here $\mathbf{r}_i(t)$ denotes the coordinates of the backbone C_α atom i at a time t, $\mathbf{r}_i(0)$ is the initial coordinate of the same atom at $t = 0$, and N is the total number of backbone C_α atoms. We define the intraprotein H-bond using the following criteria:[84] (a) a heavy atom (donor) is bonded to a hydrogen atom and another heavy atom (acceptor) is within 0.35 nm from the donor, and (b) an angle between the hydrogen-donor−acceptor is less than 30° (we used GROMACS tools for these analyses).

Figure 2g and h show the evolution of RMSD and the number of H-bonds, respectively, for the same simulation runs (black and green lines correspond to cases A and C, respectively, with the symbols e and f corresponding to the snapshots in the middle row, case C). These results show that for the high copolymer concentration (case A) the system remains structurally stable: the values of RMSD remains low and the number of H-bonds remains high.[42] Notably, both these values remain close to the same characteristics for the native enzymes at 300 K (Figure S2a,b, Supporting Information). On the contrary, both the characteristics for case C strongly deviate from their initial values. Note that the onset of the increase in RMSD and of the decrease in the number of interprotein H-bonds can be seen after 30 ns (Figure 2g and h, respectively, green lines). Recall that 30 ns is the time instant when the protein is immersed into the water phase (Figure 2e). Hence, our results show that the fraction of water in the vicinity of the protein has a critical influence on the 3D conformation of the protein. Notably, the water available at high temperature (600 K) can penetrate protein's hydrophilic outer surface and is known to result in unfolding of native proteins.[74,85] Further below we calculate a number of protein−water contacts as well as protein-triad contacts in all the simulations scenarios.

Increased Water Concentration Increases Fluctuations. We characterize the time evolution of the enzymes in both cases by using the Dictionary of Secondary Structure in Proteins (DSSP)[86] to assess the evolution of the secondary structures (Figures 3a,b). DSSP plots confirm our observations in Figure 2 that while in case A the secondary structures remain mainly intact, these structures are strongly disrupted in case C and are completely lost at 200 ns for a chosen simulation. The latter is apparent from the comparison between the DSSP plots for both cases (Figure 3, top row). While in case A all the residues remain largely intact (as represented by long horizontal stripes) for the entire length of simulations (250 ns), in case C, the β-sheets (red horizontal stripes) are disrupted at 30 ns, and the α-helices (blue horizontal stripes) are disrupted following the disruption of the β-sheets at about 100 ns. As seen in Figure 2e, lysozyme is effectively pulled into the water phase at 30 ns, and some disruption of β-sheets is also observed at the same time. Thus, the exposure to water at high temperatures correlates with the disruption of the β-sheets.

While RMSD captures the deviation of the entire protein from its initial conformation, the root−mean−square fluctuation (RMSF) quantifies the local variations in the coordinates of atoms within each residue during a chosen time frame. RMSF of a given residue ($\mathcal{R}$) is calculated as a square root of the variance of the fluctuations around its average position and is defined as

DOI: 10.1021/acs.biomac.8b00027
Biomacromolecules 2018, 19, 1175−1188

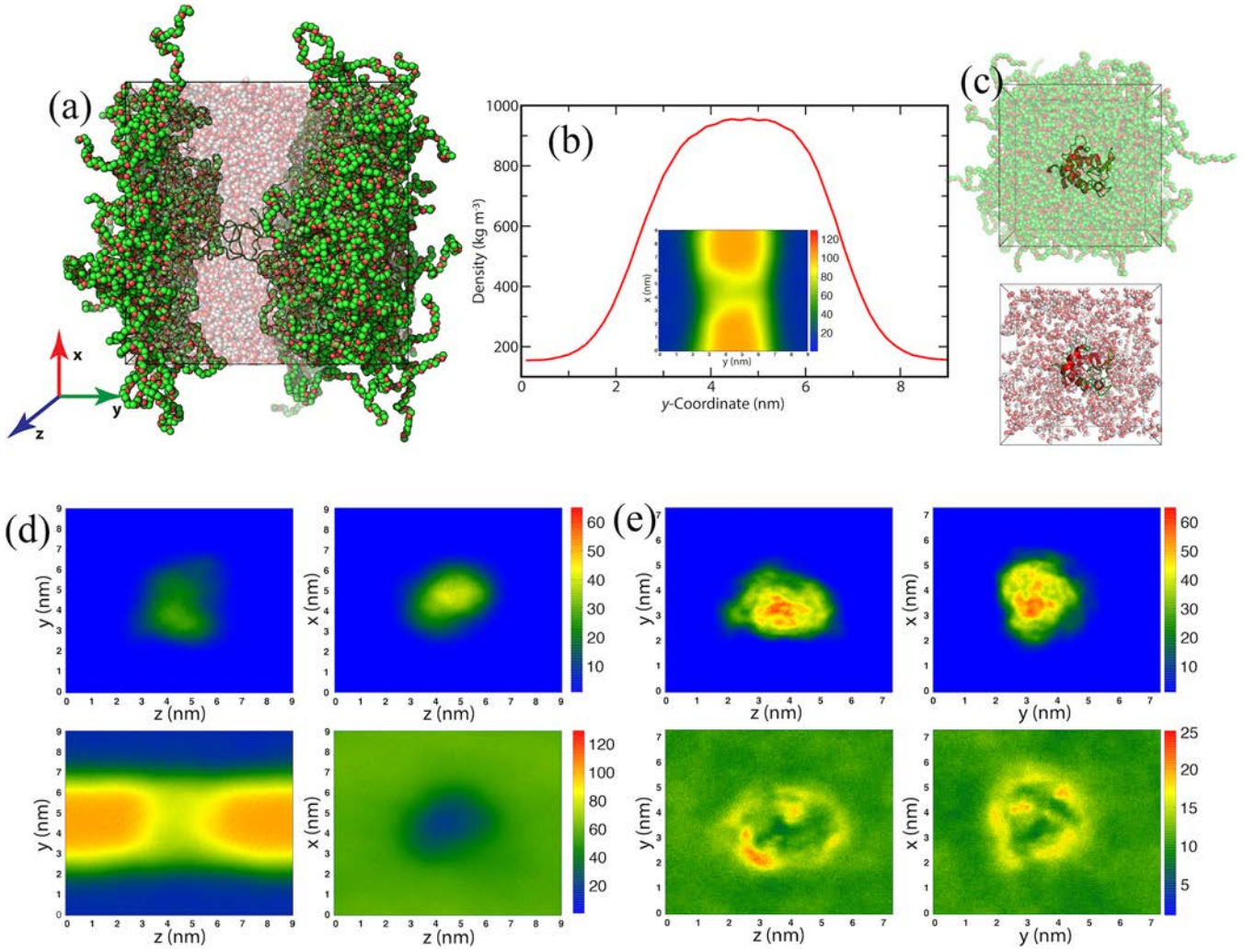

Figure 4. (a) Case C: snapshot at 200 ns. Lysozyme is shown in stick representation; water molecules are shown in pink (oxygen atoms) and gray (hydrogen atoms). (b) Density of water along the interface (y-axis) for the snapshot in panel (a) is averaged over the last 50 ns. Inset in panel b shows the number density (per nm^3) of water molecules in the $x-y$ plane. The maximum concentration of water absorbed by the triads is 163 ± 10 kg m^{-3}. (c) Case A: snapshots at 200 ns, showing only the triads (above) and only water around lysozyme. (d) Number density (per nm^3) of lysozyme (top) and water molecules (bottom) for case C in $y-z$ and $x-z$ plane. (e) Number density (per nm^3) of lysozyme (top) and water molecules (bottom) for case A system in $y-z$ and $x-y$ plane.

$$\text{RMSF}\ (\mathcal{R}) = \left[\frac{1}{T}\sum_{t=1}^{T}\left[\frac{1}{N_{\mathcal{R}}}\sum_{i=1}^{N_{\mathcal{R}}}(\mathbf{r}_i(t) - \langle\mathbf{r}_i\rangle)^2\right]\right]^{1/2} \quad (2)$$

where $\mathbf{r}_i(t)$ is the position of an atom within the residue $\mathcal{R}$ at time t after superposition on the reference structure. T is time over which the RMSF is calculated, $N_{\mathcal{R}}$ is the number of atoms within the residue $\mathcal{R}$, <···> denotes an average over atoms $N_{\mathcal{R}}$ within the residue $\mathcal{R}$. The light blue and light red shaded regions in Figure 3c and d mark α-helices and β-sheets, respectively, as originally present in the crystal structure. While for case A, the fluctuations of all the residues remain low at all times (RMSF is below 0.3 nm on average, Figure 3c), for case C, the RMSF begins to increase significantly at relatively early times (at about 30 ns, see black curve in Figure 3d). Recall that the lysozyme is separated from the copolymer matrix into the water phase at about the same instant in time in this simulation run (Figure 2e, see also Figure 4a−e discussed below).

These calculations confirm that once lysozyme is exposed to water, the β-sheets begin to disrupt (Figure 3d) so that during 100−110 ns time frame, the fluctuations of the residues are further increased (Figure 3b). Here, the β-sheets regions undergo larger scale fluctuations than the α-helices since they are already disrupted, while at 240−250 ns both regions that were formerly α-helices and β-sheets undergo large-scale fluctuations, leading to the unfolding of the lysozyme. The DSSP plots (Figure S3 of Supporting Information) for four sets at 500 K for case B and case C show that the β-sheets are prone to early disruption similar to that found in prior studies[52,66] (we note, however, that in different scenarios, helixes being disrupted earlier than β-sheets have also been reported[59]).

Phase Separation at High Temperatures. In case A, in which the secondary structures remain stable, the volume fraction of water is significantly lower than that in case C and thus water molecules have a lower probability of coming into the direct contact with the enzyme. Hence, our results indicate that preventing a water access is the underlying reason for the improved structural stability of the enzyme at high temperatures in our experimental studies.[42] Notably, for the chosen PEG to GMA ratio, the triads are miscible with water at 300 K

DOI: 10.1021/acs.biomac.8b00027
Biomacromolecules 2018, 19, 1175−1188

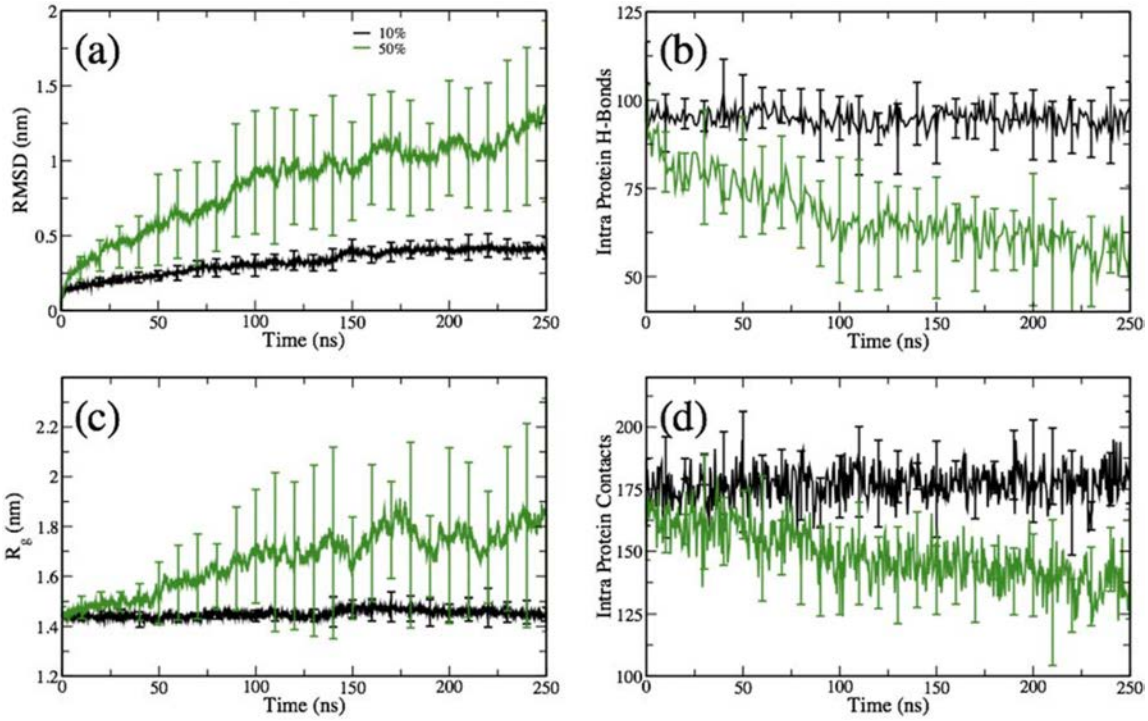

Figure 5. (a) Root−mean−square deviation (RMSD), (b) number of intra protein H-bonds, (c) radius of gyration, and (d) number of intraprotein contacts. Black and green lines are for case A and case C, respectively. The error bars represent an average over the four independent runs.

(while GMA is hydrophobic, PEG is hydrophilic at this temperature, long PEG chains prevent GMA from clustering). However, it is known that at high temperatures PEG becomes immiscible with water.[78,79,87] In our simulations, we observe the phase-separation between the triads and water at high temperatures in both case B and case C. In case A, we do not observe phase-separation between the water and triads due to the small volume fraction of water; in this case, the water molecules remain roughly uniformly distributed within the system as we show below.

The phase-separation between the water and the triads at later times can be clearly seen in Figure 4a (as well as in Figure 2e,f). To reach this stage, the smaller domains (as in Figure 2d) coarsen so that in the simulation shown in Figure 4a we observe a single pure water domain and another domain that contains predominantly triads but also a small fraction of water. The enzyme is located within the water domain with the conjugated triads buried into the copolymer phase (recall that there are six triads conjugated to lysine residues of lysozyme). In Figure 4b, we plot the water density profile along the y-axis within the simulation box; the data are averaged over the time interval of 200−250 ns. This density profile (Figure 4b) shows high density at the center of the y-axis (948 ± 9 kg m^{-3}) and a low density of approximately 163 ± 10 kg m^{-3} within the copolymer domain. Because triads are phase separated from the bulk of the water domain, this concentration can be referred to as a maximum concentration of water that can be absorbed by the triad matrix at 500 K. Thus, the triads and water would not phase separate at water concentration below 163 ± 10 kg m^{-3}. These results indicate that any water concentration above this limit would result in some degree of protein unfolding depending on the size of water domain surrounding the protein, while any water concentration below this limit would result in maintaining protein's structural stability at high temperatures.

The 2D number density profile (inset in Figure 4b) shows the distribution of water molecules in the simulation box; the density of water in the center of the box is lower as compared to that in the top and bottom regions. This central region is occupied by the lysozyme (Figure 4d, top panel). The distributions of water along the $y-z$ and $z-x$ planes are shown in Figure 4d (bottom images); here again the data are averaged over the remaining coordinate (over x and over y coordinates, respectively, for the $y-z$ and $z-x$ planes, and over the last 50 ns of simulations). Within the $z-x$ plane, the water density is low in the center since the center is occupied by the lysozyme (Figure 4d, bottom right image). Top images in Figure 4d show the distribution of lysozyme density at the same conditions; here the blue color corresponds to zero density of the enzyme.

Figure 4e shows the enzyme (top row) and water (bottom row) number density averaged over the last 50 ns for case A at the same conditions as in case C. By comparing the two panels, we can conclude that (a) the average number density of the protein remains higher in case A than in case C (as can be seen from the bright orange color in the latter case corresponding to the unfolded protein); (b) water number density is roughly uniform far from the lysozyme or from the center of the box in case A (green color in the bottom row in Figure 4e). This water number density corresponds to approximately 100 kg m^{-3} water density (far from the protein) and is lower than the critical concentration defined above. Hence, no phase separation is observed in this system; this confirms our hypothesis that the water concentration below the critical value promotes thermal stability in our system.

Effect of Concentration of Copolymer on LPC Stability at High Temperatures: General Trends. Until now we have focused on the details of two examples of dynamics during a single simulation run for case A (highest copolymer content considered herein, or 10% w/w of water) and case C (lowest

DOI: 10.1021/acs.biomac.8b00027
Biomacromolecules 2018, 19, 1175−1188

Table 2a. Number of H-Bonds for Native Lysozyme and 0%, Case A (10% w/w), Case B (30% w/w), and Case C (50% w/w) LPC Systems, Averaged over Last 50 ns of Trajectories (from 200 to 250 ns)

			LPC			
	H-bonds	native	0%	case A (10% w/w)	case B (30% w/w)	case C (50% w/w)
300 K	intraprotein	96.34	120.98	105.51	99.14	98.81
	protein−water	272.74		173.74	223.32	244.91
	protein-triads		55.59	21.97	13.44	10.22
500 K	intraprotein	52.24	113.14	95.25	57.42	56.66
	protein−water	292.23		141.82	254.84	264.15
	protein-triads		39.22	13.84	8.68	6.68

Table 2b. Number of Contacts for Native Lysozyme and 0%, Case A (10% w/w), Case B (30% w/w), and Case C (50% w/w) LPC Systems, Averaged over Last 50 ns of Trajectories (from 200 to 250 ns)

			LPC			
	contacts	native	0%	case A (10% w/w)	case B (30% w/w)	case C (50% w/w)
300 K	intraprotein	159.13	200.14	170.27	159.92	159.84
	protein−water	224.79		119.08	169.99	190.68
	protein-triads		114.61	74.97	61.96	57.59
500 K	intraprotein	128.15	206.08	180.28	139.12	129.24
	protein−water	279.48		114.23	231.62	248.84
	protein-triads		105.23	69.46	59.94	57.16

copolymer content considered in our simulations, or 50% w/w of water). To confirm that the above observations are robust and to further characterize this system, we performed four independent simulations with four different initial configurations.

RMSD, Intraprotein Hydrogen Bonds, and Radius of Gyration, R_g. Figure 5a and b show the time evolution of the RMSD and the number of intraprotein H-bonds averaged over four independent runs, respectively. These results confirm that a high degree of structural stabilization is achieved for case A (curves marked in black) as evident from the low values of RMSD and correspondingly high values of intraprotein H-bonds. On the contrary, high values of RMSD for case C confirm large-scale deviations of the protein conformation from its initial structure. These results are supported by the DSSP plots (Figure S3a-d of Supporting Information) that clearly show the disruption of β-sheets at relatively early times followed by the disruption of α-helixes at high temperatures in all four simulation runs.

We now also calculate the radius of gyration, R_g, of the protein (Figure 5c), measured as a root−mean−square distance of each atom of the protein to its center of mass:

$$R_g = \left[\frac{1}{M}\sum_{i}^{N} m_i(\mathbf{r}_i - \mathbf{r}_{cm})^2\right]^{1/2} \quad (3)$$

where M is the total mass of the protein, $\mathbf{r}_{cm}$ is the center-of-mass position of the protein, m_i is a mass of an atom i, and N is the total number of atoms within the protein. We note that while the error bars for R_g and RMSD are small for case A, indicating that the dynamics follows nearly identical path for all the simulation runs, the error bars are large for case C. The reason for this is that the unfolding depends on the location of the protein with respect to the water−copolymer domains as discussed above and hence to some degree depends on the specifics of the dynamics of the phase separation and particular initial conditions in the system. The onset of unfolding was observed at different simulation times for the runs in case C (Figure S4a of Supporting Information); further, in one out of four simulation runs, the enzyme was trapped within the copolymer domain, which prevented unfolding until the velocities were reinitialized (Figure S4b of Supporting Information, green line). The low average RMSD value for case A indicates that the native secondary conformations are preserved to a large degree and correspondingly the average R_g is maintained at a value close to its initial value (1.46 ± 0.01 nm at 250 ns). In case C, the size of the protein significantly increases during the unfolding so that R_g is 1.78 ± 0.01 nm at 250 ns (Figure 5c).

The increase in R_g and high RMSD values can be contributed to the breaking of the intraprotein H-bonds as evident from comparison between the green curves in Figure 5b and in Figure 5c, respectively, which shows that R_g (as well as RMSD) begins to increase at the same instant in time when the number of intraprotein H-bonds begins to decrease. The formation of the secondary structures such as α-helix, 3_{10}-helix and β-sheets is a result of formation of H-bonds between the acceptor and donor groups of the amino acids.[88] The intraprotein H-bonds predominantly originate from the electrostatic interaction between these polar groups.[88] The number of intraprotein H-bonds for case A remains higher for all simulations than that for case C (Figure 5b, Table 2a). The number of intraprotein H-bonds remains at 95 ± 3 for case A, while this number decreases to 66 ± 11 for case C around 100 ns (at this time, RMSD reaches a value close to unity, indicating large deviations from the initial structure corresponding to the unfolding). In other words, during the unfolding, about 30 intraprotein H-bonds are broken.[58]

Intraprotein Contacts. We now calculate a number of intraprotein contacts by counting the number of pairs of heavy atoms of lysozyme (by "heavy atoms", we refer to all the atoms except hydrogen atoms[68]) separated by the distance not exceeding 0.31 nm. Effectively, these contacts include both the electrostatic and the hydrophobic interactions. The number of intraprotein contacts for case A remains high throughout the simulations (170 ± 1), while for case C this number decreases consistently with an increase in RMSD and at around 100 ns, it is 147 ± 12 (Figure 5d, see Table 2b). The RMSD and R_g plots

DOI: 10.1021/acs.biomac.8b00027
Biomacromolecules 2018, 19, 1175−1188

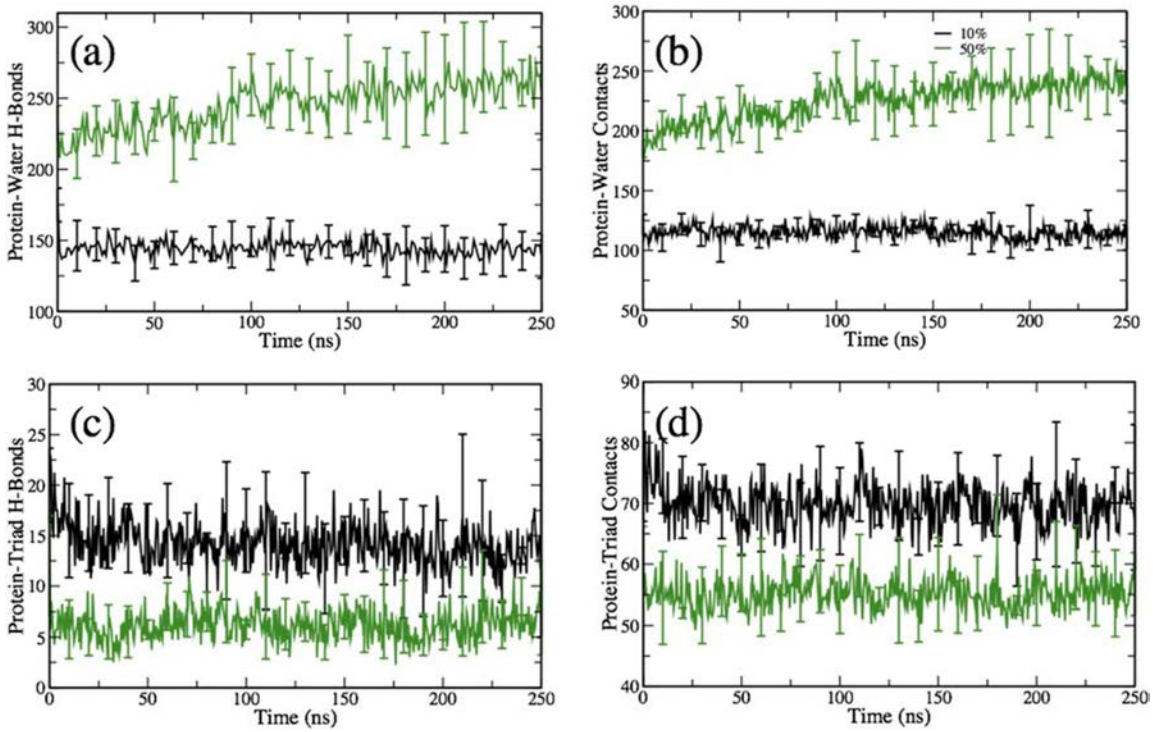

Figure 6. (a) Number of protein−water H-bonds, (b) number of protein−water contacts, (c) number of protein−triad H-bonds, and (d) number of protein−triad contacts. Black and green lines are for case A and case C, respectively. The error bars represent an average over the four independent runs.

show that the lysozyme unfolds at late times, which results in decrease of the intraprotein contacts. Comparing all the analysis in Figure 5 with the corresponding plots for the native lysozyme (Figures S2, S6 of Supporting Information), we conclude that the dynamics and the late time values of RMSD and R_g for the native lysozyme at 500 K are similar to the values calculated for case C, while the values for native enzymes at 300 K (RMSD and R_g are at 0.15 and 1.42 nm, respectively, see Figure S6a,b of the Supporting Information) are close to the same values for case A.

Notably, a number of intraprotein H-bonds and contacts for case A (Figure 5b,d, black lines) are similar to that of the native lysozyme at 300 K (Figures S2b and S6b, black lines) (∼100 and ∼160 intraprotein H-bonds and contacts, respectively) (Tables 2a and 2b). Finally, a comparison of the evolution of the secondary structures for case A at 500 K and native lysozyme at 300 K are plotted in Figure S7 of Supporting Information. All the characterizations above show a clear effect of high concentration of triads on structural stabilization of the protein for case A. In this case, the protein is mostly confined by the triads, this confinement effectively reduces the conformational entropy of the unfolded state and promotes the stabilization of the folded state. The stabilization of the folded state of proteins by crowing and confinement are supported by number of prior studies.[89−92]

Hence, our simulations show that the overall copolymer-to-water ratio plays a crucial role to ensure the stability of the secondary structures. In case C (high water concentration) at 500 K, we observe an onset of unfolding once a significant amount of water is in the contact with the enzyme. For example, in two cases shown in Figure S3a,d of Supporting Information, water and triads phase-separation occurs with the enzyme being located within the large water domain (same scenario as discussed in Figure 2d−f). Once the enzyme is surrounded by water, the unfolding process begins similar to that for the native lysozyme. Notably, in one out of four simulations (Figure S3b, Supporting Information), the enzyme unfolding was initiated, while the enzyme was primarily immersed within the copolymer phase; however, an analysis of this scenario (see Figure S8, Supporting Information) confirmed that there is a sufficiently high density of water in the vicinity of enzyme before the initiation of unfolding. Finally, in one out of four simulations (Figure S3c of Supporting Information), the secondary structure remained stable until 230 ns. The β-sheets began disrupting around 230 ns with the density plots showing an increase in water density in the vicinity of enzyme; reinitiating velocities and running the same simulation for a longer time results in unfolding (Figure S4 of Supporting Information).

Protein−Water Interactions. In pure water, protein folds with burying its hydrophobic residues and exposing hydrophilic residues to surrounding water. In cases considered herein, protein is surrounded by the mixture of water molecules and triads. It is instructive to calculate the time evolution of the number of H-bonds forming between the protein and surrounding environment and to separate the contributions from the water and from the triads. First, we focus on protein−water interactions and compute the number of protein−water H-bonds (Figure 6a) and protein−water contacts (Figure 6b). We define the protein−water contacts as a number of pairs of backbone heavy atoms (all atoms except hydrogen) and oxygen of water molecules separated by the distance not exceeding 0.31 nm (see Figure S5 of Supporting Information).

As anticipated, a number of protein−water H-bonds for case C is higher than that for case A at the onset of the simulations due to the higher water content and increases with time as

DOI: 10.1021/acs.biomac.8b00027
Biomacromolecules 2018, 19, 1175−1188

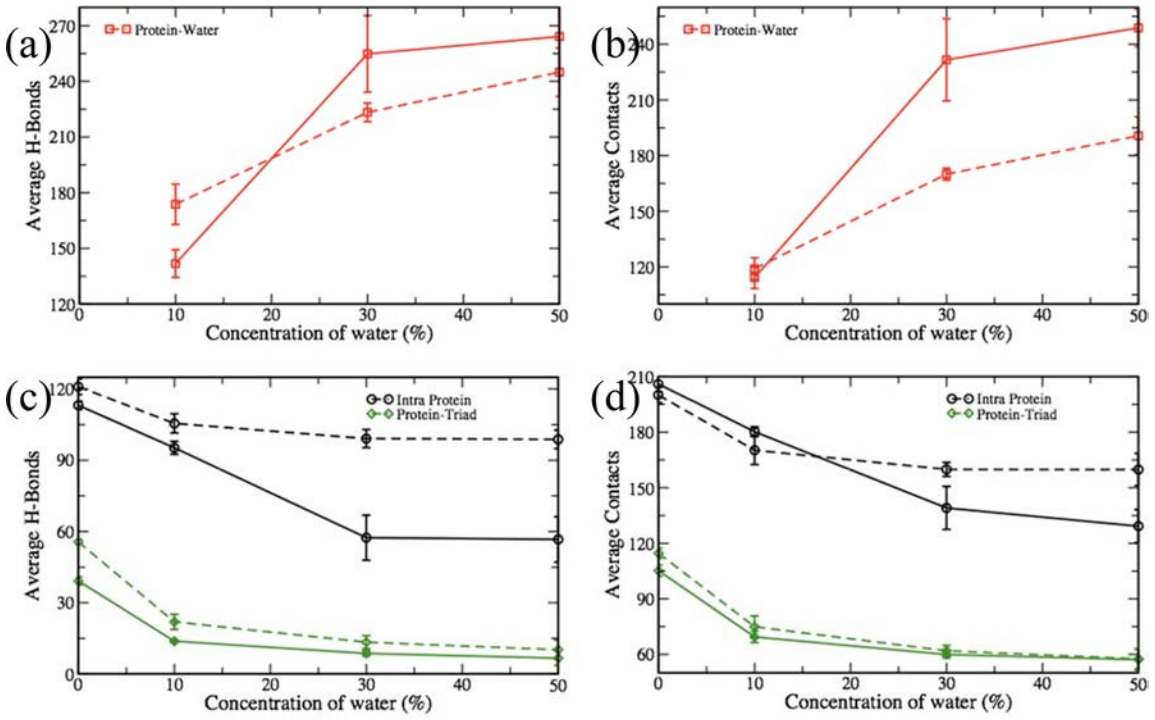

Figure 7. Average number of (a, c) H-bonds and (b, d) contacts computed from the last 10 ns of respective trajectories (from 240 ns until 250 ns). Dotted and solid lines are for 300 and 500 K, respectively. Circles, squares, and diamonds represent intraprotein, protein−water, and protein−triad, respectively. All points are averaged over four simulation trajectories. The average protein−water numbers of H-bonds for native lysozyme at 300 and 500 K are 272 and 292, respectively, and intraprotein values are 96 and 52, respectively. The average protein−water contacts at 300 and 500 K are 224 and 279, respectively, and intraprotein contacts are 159 and 128, respectively (see Tables 2a and 2b).

protein unfolds (Figure 6a, green line). The number of protein−water H-bonds in case A remains constant throughout the entire simulation (Figure 6a, black line). The protein−water contacts also show similar trends (Figure 6b); while the number of protein−water contacts remains constant for case A, it increases with time for case C.

We emphasize that while the late time increase in the protein−water contacts is due to the protein unfolding and increase in its surface area (compare the plot in Figures 6b and 5c, green lines), there is also an increase in the number of protein−water contacts at early times (roughly below 30 ns). This increase corresponds to the protein been predominantly surrounded by the water domain as we showed above.

Protein-Triad Interactions. We now calculate the number of protein-triad H-bonds and protein-triad contacts (Figure 6c,d). We define protein-triad contacts as a number of pairs of all the atoms of protein and triads excluding hydrogen atoms separated by the distance not exceeding 0.31 nm (see Figure S5 of Supporting Information). Our results show that both the number of H-bonds and the number of contacts remain constant throughout the simulation (Figures 6c,d). Both the values are higher for case A (black lines in Figure 6a,b) than the corresponding values for case C system (green lines in Figure 6c,d), as expected for the system with significantly higher copolymer content. Notably, the number of protein-triad contacts and H-bonds remains constant for case C as protein unfolds. This further indicates that the protein is primarily surrounded by water and that the triads that are conjugated with the protein provide a major contribution to the protein-triad H-bonds and contacts count. Furthermore, by separately accounting for the interactions of hydrophilic and hydrophobic residues of protein (based on the hydropathy scale by Kyte and Doolittle[93]) with triads and water, we show that most of the H-bonds form between the triads and the hydrophilic amino acids (Figure S9 of Supporting Information).

Effect of Water Concentration. Simulation studies above show that water concentration plays a critical role in maintaining structural stability of the lysozyme at high temperature. We now summarize all the cases considered in our simulations, including a case of intermediate copolymer concentration (case B) and a water-free case. Figure 7a and b show a number of protein−water H-bonds and contacts, respectively, as a function of water concentration, while Figure 7c and d show a number of intraprotein and protein-triad H-bonds and contacts, respectively. In all the cases, dashed lines correspond to T = 300 K and solid lines correspond to T = 500 K simulations. We analyzed the last 10 ns of the 250 ns simulation trajectories and averaged over four independent runs. The number of protein−water H-bonds at 500 K increases drastically from 143 ± 3 for 10% of water (case A) to 231 ± 10 for 30% of water (case B); further increase with the increase in fraction of water is less pronounced (248 ± 22 for 50% of water, case C) (Figure 7a). The number of protein−water contacts has similar trends. Note that the same number of protein−water contacts at low and high temperatures (lowest point on Figure 7b for 10% of water) indicates that the protein structure at high temperatures remains similar to that at 300 K. A significantly higher number of contacts for both 30% and 50% of water at 500 K than that at 300 K is attributed to the unfolding of the protein and correspondingly a greater fraction of the heavy atoms of protein backbone exposed to surrounding water. The number of intraprotein H-bonds at 500 K also shows a greater decrease from 10% of water (95 ± 3) to 30% of water (72 ± 6) and a less pronounced decrease for 50% of

DOI: 10.1021/acs.biomac.8b00027
Biomacromolecules 2018, 19, 1175−1188

water (66 ± 11). The number of protein-triad H-bonds decreases dramatically between the water-free and 10% of water system; further decrease in this number is less pronounced (green lines in Figure 7c,d). The number of intraprotein and protein−triad contacts exhibit the same trends as the corresponding H-bonds (Figure 7d). Importantly, the numbers of H-bonds and intraprotein contacts are the highest for the water-free case (black lines in Figure 7c,d); these numbers exceed the same numbers for the native protein at 300 K (see Figure S10 of Supporting Information) indicating high structural stability of protein immersed into the pure mixture of triads. Notably, our results are consistent with the findings from the prior experimental study demonstrating recovery of lysozyme activity up to 78 ± 9% after heat treatment at 90 °C only at highly concentrated polymer solution.[42] To summarize, these results show a relatively small difference between all the high temperature characteristics (H-bonds and number of contacts) for cases B and C, indicating that only case A remains effective in reducing the accessibility of water to lysozyme, which in turn results in preserving its secondary structure.[25,40] Our results show that the underlying reason for such high thermal stability is the absence of phase separation at this low fraction of water so that the pure water domains are no longer formed in the vicinity of the enzyme (these water domain initiate unfolding in remaining scenarios, cases B and C).

We note that in our simulations we vary the copolymer/water concentration in our simulation box so that we can probe the effects of different concentrations on the dynamics of the conjugate. In our experiments, using a dynamic light scattering method, we also observe densification of the copolymer shell in the close vicinity of the enzyme.[42] The atomic force microscopy experiments for the visualization of the conjugate structure in the dry state after removal of water revealed compactization of the conjugate with respect to the unconjugated copolymer structure. Further experiments will be conducted to characterize changes in the conjugates structures with concentration of the copolymer.

CONCLUSIONS

Enhancing thermal stability of enzymes could benefit a range of applications from food processing[1] to enzyme enhanced oil recovery applications.[5,6] We employed molecular dynamics simulations to explore the dynamics and structural stability of lysozyme−poly(GMA-*stat*-OEGMA) conjugate at elevated temperature by varying the copolymer/water content. Our results show that for all the cases with relatively high water content (cases B and C), the phase separation and formation of the water domains and copolymer-rich domains is observed at high temperature. In all these scenarios, the lysozyme becomes exposed to the water domains, which we quantified by an increase in the number of H-bonds and contacts between the water molecules and the lysozyme. This leads to the disruption of secondary structures and, thus, melting of lysozyme. Notably, in all the above cases, at late simulation times, the secondary structures are lost.

On the contrary, no phase separation is observed at the highest polymer concentration considered herein (case A), and the enzyme's secondary structures remain largely intact with respect to the native structures at an ambient temperature. The structural stability analysis (RMSD, number of intraprotein H-bonds and contacts) shows that the lysozyme retained its structural integrity in response to a temperature increase. For the cases B and C, however, the RMSD increases, and both the numbers of intraprotein H-bonds and intraprotein contacts decrease upon the contact of the protein with the water domain.

Hence, our results show that the dynamics of phase separation in the water−copolymer system surrounding the enzyme is critical for the structural stability of the enzyme and that the contact between the water domain and the enzyme marks the onset of unfolding. These results are consistent with the prior studies highlighting an importance of maintaining a low water content in the vicinity of lysozyme to promote its structural stability under different conditions. For example, recovery of lysozyme activity up to ∼80% after heat treatment at 90 °C was observed only in highly concentrated polymer solutions[94] and for sufficiently long PEG chains densely bound to soft nanotube channels,[95] while essentially no recovery of lysozyme activity was observed at lowest polymer concentrations or shorter polymer chains, respectively, at the same conditions. As another example, PEG chains forming an effective barrier for the surrounding water molecules around a PEGylated peptide were shown to prolong the onset of unfolding events and improve the mechanical stability of the conjugates.[21]

In our studies, we identified a critical concentration of water (163 ± 10 kg m^{-3}) in the water−polymer mixture, below which the phase separation is no longer observed and the enzyme remains structurally stable at elevated temperature. The simulations in case A considered herein correspond to the water concentration below this limit. Our results point out to the critical role the densification of the cocoons enveloping the enzymes plays[42] in the resulting thermal stability of these enzymes observed in our experimental studies. This understanding provides a basis for future studies on designing a range of enzyme−copolymer conjugates with improved stability.

ASSOCIATED CONTENT

Supporting Information

The Supporting Information is available free of charge on the ACS Publications website at DOI: 10.1021/acs.biomac.8b00027.

Additional simulation details and tables listing force field parameters; data of RMSD, intra protein H-bonds, radius of gyration, number of intraprotein contacts, number of protein−water H-bonds, and number of protein−water contacts; radial distribution, 2D number density, number of H-bonds and contacts (PDF)

AUTHOR INFORMATION

Corresponding Author

*E-mail: okuksen@clemson.edu.

ORCID

Igor Luzinov: 0000-0002-1604-6519
Sergiy Minko: 0000-0002-7747-9668
Olga Kuksenok: 0000-0002-1895-5206

Notes

The authors declare no competing financial interest.

ACKNOWLEDGMENTS

O.K. gratefully acknowledges the donors of the American Chemical Society Petroleum Research Fund (No. 56632-ND7) for partial funding of CKC and National Science Foundation EPSCoR Program Award No. OIA-1655740 for partial funding

DOI: 10.1021/acs.biomac.8b00027
Biomacromolecules 2018, 19, 1175−1188

of ST. S.M. acknowledges NSF Award No. 1604526. Clemson University is acknowledged for generous allotment of compute time on Palmetto cluster.

REFERENCES

(1) Vieille, C.; Zeikus, G. J. Hyperthermophilic Enzymes: Sources, Uses, and Molecular Mechanisms for Thermostability. *Microbiol. Mol. Biol. Rev.* **2001**, *65* (1), 1−43.
(2) Iyer, P. V.; Ananthanarayan, L. Enzyme stability and stabilization—Aqueous and non-aqueous environment. *Process Biochem.* **2008**, *43* (10), 1019−1032.
(3) D'Haeseleer, P.; Gladden, J. M.; Allgaier, M.; Chain, P. S. G.; Tringe, S. G.; Malfatti, S. A.; Aldrich, J. T.; Nicora, C. D.; Robinson, E. W.; Paša-Tolić, L.; Hugenholtz, P.; Simmons, B. A.; Singer, S. W. Proteogenomic Analysis of a Thermophilic Bacterial Consortium Adapted to Deconstruct Switchgrass. *PLoS One* **2013**, *8* (7), e68465.
(4) Gupta, D. V. S.; Prasek, B. B.; Horn, R. D. *Enzyme breakers for breaking fracturing fluids and methods of making and use thereof*. U.S. Grant US5441109A,1995.
(5) McCutchen, C. M.; Duffaud, G. D.; Leduc, P.; Petersen, A. R. H.; Tayal, A.; Khan, S. A.; Kelly, R. M. Characterization of extremely thermostable enzymatic breakers (α-1,6-galactosidase and β-1,4-mannanase) from the hyperthermophilic bacterium Thermotoga neapolitana 5068 for hydrolysis of guar gum. *Biotechnol. Bioeng.* **1996**, *52* (2), 332−339.
(6) Patel, J.; Borgohain, S.; Kumar, M.; Rangarajan, V.; Somasundaran, P.; Sen, R. Recent developments in microbial enhanced oil recovery. *Renewable Sustainable Energy Rev.* **2015**, *52*, 1539−1558.
(7) Hesampour, A.; Siadat, S. E. R.; Malboobi, M. A.; Mohandesi, N.; Arab, S. S.; Ghahremanpour, M. M. Enhancement of Thermostability and Kinetic Efficiency of Aspergillus niger PhyA Phytase by Site-Directed Mutagenesis. *Appl. Biochem. Biotechnol.* **2015**, *175* (5), 2528−2541.
(8) Mao, S.; Gao, P.; Lu, Z.; Lu, F.; Zhang, C.; Zhao, H.; Bie, X. Engineering of a thermostable β-1,3−1,4-glucanase from Bacillus altitudinis YC-9 to improve its catalytic efficiency. *J. Sci. Food Agric.* **2016**, *96* (1), 109.
(9) Cui, J.; Liang, L.; Han, C.; lin Liu, R. Stabilization of Phenylalanine Ammonia Lyase from Rhodotorula glutinis by Encapsulation in Polyethyleneimine-Mediated Biomimetic Silica. *Appl. Biochem. Biotechnol.* **2015**, *176* (4), 999−1011.
(10) Zhang, D.-H.; Peng, L.-J.; Wang, Y.; Li, Y.-Q. Lipase immobilization on epoxy-activated poly(vinyl acetate-acrylamide) microspheres. *Colloids Surf., B* **2015**, *129*, 206−210.
(11) Hermanova, S.; Zarevucka, M.; Bousa, D.; Pumera, M.; Sofer, Z. Graphene oxide immobilized enzymes show high thermal and solvent stability. *Nanoscale* **2015**, *7* (13), 5852−5858.
(12) Srivastava, G.; Singh, K.; Talat, M.; Srivastava, O. N.; Kayastha, A. M. Functionalized Graphene Sheets As Immobilization Matrix for Fenugreek β-Amylase: Enzyme Kinetics and Stability Studies. *PLoS One* **2014**, *9* (11), e113408.
(13) Yin, Y.; Xiao, Y.; Lin, G.; Xiao, Q.; Lin, Z.; Cai, Z. An enzyme-inorganic hybrid nanoflower based immobilized enzyme reactor with enhanced enzymatic activity. *J. Mater. Chem. B* **2015**, *3* (11), 2295−2300.
(14) Sohrabi, N.; Rasouli, N.; Torkzadeh, M. Enhanced stability and catalytic activity of immobilized α-amylase on modified Fe3O4 nanoparticles. *Chem. Eng. J.* **2014**, *240*, 426−433.
(15) Sun, X.; Cai, X.; Wang, R.-Q.; Xiao, J. Immobilized trypsin on hydrophobic cellulose decorated nanoparticles shows good stability and reusability for protein digestion. *Anal. Biochem.* **2015**, *477*, 21−27.
(16) Cummings, C.; Murata, H.; Koepsel, R.; Russell, A. J. Dramatically Increased pH and Temperature Stability of Chymotrypsin Using Dual Block Polymer-Based Protein Engineering. *Biomacromolecules* **2014**, *15* (3), 763−771.
(17) Gizurarson, J. G. K.; Filippusson, H. Conjugation of d-glucosamine to bovine trypsin increases thermal stability and alters functional properties. *Enzyme Microb. Technol.* **2015**, *75*−*76*, 1−9.
(18) Suthiwangcharoen, N.; Nagarajan, R. Enhancing Enzyme Stability by Construction of Polymer−Enzyme Conjugate Micelles for Decontamination of Organophosphate Agents. *Biomacromolecules* **2014**, *15* (4), 1142−1152.
(19) Mozhaev, V. V.; Melik-nubarov, N. S.; Sergeeva, M. V.; Šikšnis, V.; Martinek, K. Strategy for Stabilizing Enzymes Part One: Increasing Stability of Enzymes via their Multi-Point Interaction with a Support. *Biocatal. Biotransform.* **1990**, *3* (3), 179−187.
(20) Lucius, M.; Falatach, R.; McGlone, C.; Makaroff, K.; Danielson, A.; Williams, C.; Nix, J. C.; Konkolewicz, D.; Page, R. C.; Berberich, J. A. Investigating the Impact of Polymer Functional Groups on the Stability and Activity of Lysozyme−Polymer Conjugates. *Biomacromolecules* **2016**, *17* (3), 1123−1134.
(21) DeBenedictis, E. P.; Hamed, E.; Keten, S. Mechanical Reinforcement of Proteins with Polymer Conjugation. *ACS Nano* **2016**, *10* (2), 2259−2267.
(22) Hamley, I. W. PEG−Peptide Conjugates. *Biomacromolecules* **2014**, *15* (5), 1543−1559.
(23) Yang, C.; Lu, D.; Liu, Z. How PEGylation Enhances the Stability and Potency of Insulin: A Molecular Dynamics Simulation. *Biochemistry* **2011**, *50* (13), 2585−2593.
(24) Jain, A.; Ashbaugh, H. S. Helix stabilization of poly(ethylene glycol)-peptide conjugates. *Biomacromolecules* **2011**, *12* (7), 2729−2734.
(25) Hamed, E.; Xu, T.; Keten, S. Poly(ethylene glycol) Conjugation Stabilizes the Secondary Structure of α-Helices by Reducing Peptide Solvent Accessible Surface Area. *Biomacromolecules* **2013**, *14* (11), 4053−4060.
(26) Kuznetsova, M. I.; Turoverov, K. K.; Uversky, N. V. What Macromolecular Crowding Can Do to a Protein. *Int. J. Mol. Sci.* **2014**, *15* (12), 23090.
(27) Ellis, R. J. Macromolecular crowding: an important but neglected aspect of the intracellular environment. *Curr. Opin. Struct. Biol.* **2001**, *11* (1), 114−119.
(28) Feig, M.; Yu, I.; Wang, P.-h.; Nawrocki, G.; Sugita, Y. Crowding in Cellular Environments at an Atomistic Level from Computer Simulations. *J. Phys. Chem. B* **2017**, *121*, 8009.
(29) Gorensek-Benitez, A. H.; Smith, A. E.; Stadmiller, S. S.; Perez Goncalves, G. M.; Pielak, G. J. Cosolutes, Crowding, and Protein Folding Kinetics. *J. Phys. Chem. B* **2017**, *121* (27), 6527−6537.
(30) Zhou, H.-X. Polymer crowders and protein crowders act similarly on protein folding stability. *FEBS Lett.* **2013**, *587* (5), 394−397.
(31) Wang, Y.; Sarkar, M.; Smith, A. E.; Krois, A. S.; Pielak, G. J. Macromolecular Crowding and Protein Stability. *J. Am. Chem. Soc.* **2012**, *134* (40), 16614−16618.
(32) Senske, M.; Törk, L.; Born, B.; Havenith, M.; Herrmann, C.; Ebbinghaus, S. Protein Stabilization by Macromolecular Crowding through Enthalpy Rather Than Entropy. *J. Am. Chem. Soc.* **2014**, *136* (25), 9036−9041.
(33) Benton, L. A.; Smith, A. E.; Young, G. B.; Pielak, G. J. Unexpected Effects of Macromolecular Crowding on Protein Stability. *Biochemistry* **2012**, *51* (49), 9773−9775.
(34) Carmichael, S. P.; Shell, M. S. Entropic (de)stabilization of surface-bound peptides conjugated with polymers. *J. Chem. Phys.* **2015**, *143* (24), 243103.
(35) Rodríguez-Martínez, J. A.; Rivera-Rivera, I.; Griebenow, K. Prevention of benzyl alcohol-induced aggregation of chymotrypsinogen by PEGylation. *J. Pharm. Pharmacol.* **2011**, *63* (6), 800−805.
(36) Plesner, B.; Fee, C. J.; Westh, P.; Nielsen, A. D. Effects of PEG size on structure, function and stability of PEGylated BSA. *Eur. J. Pharm. Biopharm.* **2011**, *79* (2), 399−405.
(37) Lawrence, P. B.; Price, J. L. How PEGylation influences protein conformational stability. *Curr. Opin. Chem. Biol.* **2016**, *34*, 88−94.

DOI: 10.1021/acs.biomac.8b00027
Biomacromolecules 2018, 19, 1175−1188

(38) Lee, L. L. Y.; Lee, J. C. Thermal stability of proteins in the presence of poly(ethylene glycols). *Biochemistry* **1987**, *26* (24), 7813−7819.
(39) Crowley, P. B.; Brett, K.; Muldoon, J. NMR Spectroscopy Reveals Cytochrome c−Poly(ethylene glycol) Interactions. *ChemBioChem* **2008**, *9* (5), 685−688.
(40) Keefe, A. J.; Jiang, S. Poly(zwitterionic)protein conjugates offer increased stability without sacrificing binding affinity or bioactivity. *Nat. Chem.* **2012**, *4* (1), 59−63.
(41) Klibanov, A. M. Improving enzymes by using them in organic solvents. *Nature* **2001**, *409* (6817), 241−246.
(42) Yadavalli, N. S.; Borodinov, N.; Choudhury, C.; Quiñones-Ruiz, T.; Laradji, A.; Tu, S.; Lednev, I.; Kuksenok, O.; Luzinov, I.; Minko, S. Thermal Stabilization of Enzymes with Molecular Brushes. *ACS Catal.* **2017**, *7* (12), 8675−8684.
(43) van Gunsteren, W. F.; Hünenberger, P. H.; Kovacs, H.; Mark, A. E.; Schiffer, C. A. Investigation of protein unfolding and stability by computer simulation. *Philos. Trans. R. Soc., B* **1995**, *348* (1323), 49.
(44) Lee, H.; Venable, R. M.; MacKerell, A. D., Jr; Pastor, R. W. Molecular Dynamics Studies of Polyethylene Oxide and Polyethylene Glycol: Hydrodynamic Radius and Shape Anisotropy. *Biophys. J.* **2008**, *95* (4), 1590−1599.
(45) Lee, S.; Tran, A.; Allsopp, M.; Lim, J. B.; Henin, J.; Klauda, J. B. CHARMM36 United Atom Chain Model for Lipids and Surfactants. *J. Phys. Chem. B* **2014**, *118* (2), 547−556.
(46) Vanommeslaeghe, K.; MacKerell, A. D. Automation of the CHARMM General Force Field (CGenFF) I: Bond Perception and Atom Typing. *J. Chem. Inf. Model.* **2012**, *52* (12), 3144−3154.
(47) Vanommeslaeghe, K.; Raman, E. P.; MacKerell, A. D. Automation of the CHARMM General Force Field (CGenFF) II: Assignment of Bonded Parameters and Partial Atomic Charges. *J. Chem. Inf. Model.* **2012**, *52* (12), 3155−3168.
(48) Frisch, M. J.; Trucks, G. W.; Schlegel, H. B.; Scuseria, G. E.; Robb, M. A.; Cheeseman, J. R.; Scalmani, G.; Barone, V.; Mennucci, B.; Petersson, G. A.; Nakatsuji, H.; Caricato, M.; Li, X.; Hratchian, H. P.; Izmaylov, A. F.; Bloino, J.; Zheng, G.; Sonnenberg, J. L.; Hada, M.; Ehara, M.; Toyota, K.; Fukuda, R.; Hasegawa, J.; Ishida, M.; Nakajima, T.; Honda, Y.; Kitao, O.; Nakai, H.; Vreven, T.; Montgomery, J. A., Jr.; Peralta, J. E.; Ogliaro, F.; Bearpark, M.; Heyd, J. J.; Brothers, E.; Kudin, K. N.; Staroverov, V. N.; Kobayashi, R.; Normand, J.; Raghavachari, K.; Rendell, A.; Burant, J. C.; Iyengar, S. S.; Tomasi, J.; Cossi, M.; Rega, N.; Millam, J. M.; Klene, M.; Knox, J. E.; Cross, J. B.; Bakken, V.; Adamo, C.; Jaramillo, J.; Gomperts, R.; Stratmann, R. E.; Yazyev, O.; Austin, A. J.; Cammi, R.; Pomelli, C.; Ochterski, J. W.; Martin, R. L.; Morokuma, K.; Zakrzewski, V. G.; Voth, G. A.; Salvador, P.; Dannenberg, J. J.; Dapprich, S.; Daniels, A. D.; Farkas, O.; Foresman, J. B.; Ortiz, J. V.; Cioslowski, J.; Fox, D. J. *Gaussian 09*; Gaussian, Inc.: Wallingford, CT, 2009.
(49) MacKerell, A. D.; Bashford, D.; Bellott, M.; Dunbrack, R. L.; Evanseck, J. D.; Field, M. J.; Fischer, S.; Gao, J.; Guo, H.; Ha, S.; Joseph-McCarthy, D.; Kuchnir, L.; Kuczera, K.; Lau, F. T. K.; Mattos, C.; Michnick, S.; Ngo, T.; Nguyen, D. T.; Prodhom, B.; Reiher, W. E.; Roux, B.; Schlenkrich, M.; Smith, J. C.; Stote, R.; Straub, J.; Watanabe, M.; Wiórkiewicz-Kuczera, J.; Yin, D.; Karplus, M. All-Atom Empirical Potential for Molecular Modeling and Dynamics Studies of Proteins. *J. Phys. Chem. B* **1998**, *102* (18), 3586−3616.
(50) Neverov, V. S.; Komolkin, A. V. A study of the structural and thermodynamic properties of water by the molecular dynamics method. *Russ. J. Phys. Chem. B* **2010**, *4* (2), 217−226.
(51) Estacio, S. G.; Martiniano, H. F. M. C.; Faisca, P. F. N. Thermal unfolding simulations of NBD1 domain variants reveal structural motifs associated with the impaired folding of F508del-CFTR. *Mol. BioSyst.* **2016**, *12* (9), 2834−2848.
(52) Eleftheriou, M.; Germain, R. S.; Royyuru, A. K.; Zhou, R. Thermal denaturing of mutant lysozyme with both the OPLSAA and the CHARMM force fields. *J. Am. Chem. Soc.* **2006**, *128* (41), 13388−95.
(53) Pande, V. S.; Rokhsar, D. S. Molecular dynamics simulations of unfolding and refolding of a β-hairpin fragment of protein G. *Proc. Natl. Acad. Sci. U. S. A.* **1999**, *96* (16), 9062.
(54) Walser, R.; Mark, A. E.; van Gunsteren, W. F. On the Temperature and Pressure Dependence of a Range of Properties of a Type of Water Model Commonly Used in High-Temperature Protein Unfolding Simulations. *Biophys. J.* **2000**, *78* (6), 2752−2760.
(55) Abraham, M. J.; Murtola, T.; Schulz, R.; Páll, S.; Smith, J. C.; Hess, B.; Lindahl, E. GROMACS: High performance molecular simulations through multi-level parallelism from laptops to supercomputers. *SoftwareX* **2015**, *1*−*2*, 19−25.
(56) Van der Spoel, D.; Lindahl, E.; Hess, B.; Groenhof, G.; Mark, A. E.; Berendsen, H. J. C. GROMACS: Fast, flexible, and free. *J. Comput. Chem.* **2005**, *26* (16), 1701−1718.
(57) Sophianopoulos, A. J.; Weiss, B. J. Thermodynamics of Conformational Changes of Proteins. I. pH-dependent Denaturation of Muramidase. *Biochemistry* **1964**, *3* (12), 1920−1928.
(58) Mark, A. E.; van Gunsteren, W. F. Simulation of the thermal denaturation of hen egg white lysozyme: trapping the molten globule state. *Biochemistry* **1992**, *31* (34), 7745−8.
(59) Hunenberger, P. H.; Mark, A. E.; van Gunsteren, W. F. Computational approaches to study protein unfolding: hen egg white lysozyme as a case study. *Proteins: Struct., Funct., Genet.* **1995**, *21* (3), 196−213.
(60) Daggett, V.; Levitt, M. Protein Unfolding Pathways Explored Through Molecular Dynamics Simulations. *J. Mol. Biol.* **1993**, *232* (2), 600−619.
(61) Tirado-Rives, J.; Jorgensen, W. L. Molecular dynamics simulations of the unfolding of apomyoglobin in water. *Biochemistry* **1993**, *32* (16), 4175−4184.
(62) Mayor, U.; Johnson, C. M.; Daggett, V.; Fersht, A. R. Protein folding and unfolding in microseconds to nanoseconds by experiment and simulation. *Proc. Natl. Acad. Sci. U. S. A.* **2000**, *97* (25), 13518−13522.
(63) Day, R.; Bennion, B. J.; Ham, S.; Daggett, V. Increasing Temperature Accelerates Protein Unfolding Without Changing the Pathway of Unfolding. *J. Mol. Biol.* **2002**, *322* (1), 189−203.
(64) Beck, D. A. C.; Daggett, V. Methods for molecular dynamics simulations of protein folding/unfolding in solution. *Methods* **2004**, *34* (1), 112−120.
(65) Purmonen, M.; Valjakka, J.; Takkinen, K.; Laitinen, T.; Rouvinen, J. Molecular dynamics studies on the thermostability of family 11 xylanases. *Protein Eng., Des. Sel.* **2007**, *20* (11), 551−559.
(66) Meersman, F.; Atilgan, C.; Miles, A. J.; Bader, R.; Shang, W.; Matagne, A.; Wallace, B. A.; Koch, M. H. Consistent picture of the reversible thermal unfolding of hen egg-white lysozyme from experiment and molecular dynamics. *Biophys. J.* **2010**, *99* (7), 2255−63.
(67) Toofanny, R. D.; Daggett, V. Understanding protein unfolding from molecular simulations. *Wiley Interdisciplinary Reviews: Computational Molecular Science* **2012**, *2* (3), 405−423.
(68) Du, X.; Sang, P.; Xia, Y.-L.; Li, Y.; Liang, J.; Ai, S.-M.; Ji, X.-L.; Fu, Y.-X.; Liu, S.-Q. Comparative thermal unfolding study of psychrophilic and mesophilic subtilisin-like serine proteases by molecular dynamics simulations. *J. Biomol. Struct. Dyn.* **2017**, *35*, 1−18.
(69) Daggett, V.; Levitt, M. A model of the molten globule state from molecular dynamics simulations. *Proc. Natl. Acad. Sci. U. S. A.* **1992**, *89* (11), 5142−5146.
(70) Daggett, V.; Levitt, M. Molecular dynamics simulations of helix denaturation. *J. Mol. Biol.* **1992**, *223* (4), 1121−1138.
(71) Vogt, G.; Argos, P. Protein thermal stability: hydrogen bonds or internal packing? *Folding Des.* **1997**, *2* (Suppl 1), S40−S46.
(72) García, A. E.; Onuchic, J. N. Folding a protein in a computer: An atomic description of the folding/unfolding of protein A. *Proc. Natl. Acad. Sci. U. S. A.* **2003**, *100* (24), 13898−13903.
(73) Fersht, A. R.; Daggett, V. Protein Folding and Unfolding at Atomic Resolution. *Cell* **2002**, *108* (4), 573−582.
(74) Caflisch, A.; Karplus, M. Molecular dynamics simulation of protein denaturation: solvation of the hydrophobic cores and

DOI: 10.1021/acs.biomac.8b00027
Biomacromolecules 2018, 19, 1175−1188

secondary structure of barnase. *Proc. Natl. Acad. Sci. U. S. A.* **1994**, *91* (5), 1746−1750.
(75) Itzhaki, L. S.; Otzen, D. E.; Fersht, A. R. The Structure of the Transition State for Folding of Chymotrypsin Inhibitor 2 Analysed by Protein Engineering Methods: Evidence for a Nucleation-condensation Mechanism for Protein Folding. *J. Mol. Biol.* **1995**, *254* (2), 260−288.
(76) Daggett, V.; Li, A.; Itzhaki, L. S.; Otzen, D. E.; Fersht, A. R. Structure of the Transition State for Folding of a Protein Derived from Experiment and Simulation. *J. Mol. Biol.* **1996**, *257* (2), 430−440.
(77) Ghosh, A.; Brinda, K. V.; Vishveshwara, S. Dynamics of Lysozyme Structure Network: Probing the Process of Unfolding. *Biophys. J.* **2007**, *92* (7), 2523−2535.
(78) Saeki, S.; Kuwahara, N.; Nakata, M.; Kaneko, M. Upper and lower critical solution temperatures in poly (ethylene glycol) solutions. *Polymer* **1976**, *17* (8), 685−689.
(79) Israelachvili, J. The different faces of poly(ethylene glycol). *Proc. Natl. Acad. Sci. U. S. A.* **1997**, *94* (16), 8378−8379.
(80) Hey, M. J.; Ilett, S. M.; Davidson, G. Effect of temperature on poly(ethylene oxide) chains in aqueous solution. A viscometric, 1H NMR and Raman spectroscopic study. *J. Chem. Soc., Faraday Trans.* **1995**, *91* (21), 3897−3900.
(81) Seibert, M. M.; Patriksson, A.; Hess, B.; van der Spoel, D. Reproducible Polypeptide Folding and Structure Prediction using Molecular Dynamics Simulations. *J. Mol. Biol.* **2005**, *354* (1), 173−183.
(82) Zhang, Z.; Zhu, Y.; Shi, Y. Molecular dynamics simulations of urea and thermal-induced denaturation of S-peptide analogue. *Biophys. Chem.* **2001**, *89* (2), 145−162.
(83) Rocco, A. G.; Mollica, L.; Ricchiuto, P.; Baptista, A. M.; Gianazza, E.; Eberini, I. Characterization of the Protein Unfolding Processes Induced by Urea and Temperature. *Biophys. J.* **2008**, *94* (6), 2241−2251.
(84) Luzar, A.; Chandler, D. Hydrogen-bond kinetics in liquid water. *Nature* **1996**, *379*, 55.
(85) Williams, M. A.; Thornton, J. M.; Goodfellow, J. M. Modelling protein unfolding: hen egg-white lysozyme. *Protein Eng., Des. Sel.* **1997**, *10* (8), 895−903.
(86) Kabsch, W.; Sander, C. Dictionary of protein secondary structure: Pattern recognition of hydrogen-bonded and geometrical features. *Biopolymers* **1983**, *22* (12), 2577−2637.
(87) Koda, Y.; Terashima, T.; Sawamoto, M. LCST-Type Phase Separation of Poly[poly(ethylene glycol) methyl ether methacrylate]s in Hydrofluorocarbon. *ACS Macro Lett.* **2015**, *4* (12), 1366−1369.
(88) Hubbard, R. E.; Kamran Haider, M. Hydrogen Bonds in Proteins: Role and Strength. *Encyclopedia of Life Science*; John Wiley & Sons, Ltd, 2001.
(89) Ravindra, R.; Zhao, S.; Gies, H.; Winter, R. Protein Encapsulation in Mesoporous Silicate: The Effects of Confinement on Protein Stability, Hydration, and Volumetric Properties. *J. Am. Chem. Soc.* **2004**, *126* (39), 12224−12225.
(90) Bolis, D.; Politou, A. S.; Kelly, G.; Pastore, A.; Andrea Temussi, P. Protein Stability in Nanocages: A Novel Approach for Influencing Protein Stability by Molecular Confinement. *J. Mol. Biol.* **2004**, *336* (1), 203−212.
(91) Perham, M.; Stagg, L.; Wittung-Stafshede, P. Macromolecular crowding increases structural content of folded proteins. *FEBS Lett.* **2007**, *581* (26), 5065−5069.
(92) Lucent, D.; Vishal, V.; Pande, V. S. Protein folding under confinement: A role for solvent. *Proc. Natl. Acad. Sci. U. S. A.* **2007**, *104* (25), 10430.
(93) Kyte, J.; Doolittle, R. F. A simple method for displaying the hydropathic character of a protein. *J. Mol. Biol.* **1982**, *157* (1), 105−132.
(94) Sadhukhan, N.; Muraoka, T.; Ui, M.; Nagatoishi, S.; Tsumoto, K.; Kinbara, K. Protein stabilization by an amphiphilic short monodisperse oligo(ethylene glycol). *Chem. Commun.* **2015**, *51* (40), 8457−8460.
(95) Kameta, N.; Matsuzawa, T.; Yaoi, K.; Masuda, M. Short polyethylene glycol chains densely bound to soft nanotube channels for inhibition of protein aggregation. *RSC Adv.* **2016**, *6* (43), 36744−36750.

DOI: 10.1021/acs.biomac.8b00027
Biomacromolecules 2018, 19, 1175−1188